

## Mitigating Voltage Fade of $0.5\text{Li}_2\text{MnO}_3 \cdot 0.5\text{LiMn}_{1/3}\text{Ni}_{1/3}\text{Co}_{1/3}\text{O}_2$ Cathode Materials Using a Mild Method for Lithium-ion Batteries

Xingping Chang, Qunjie Xu\*, Xiaolei Yuan, Chunyan Lai\*, Haimei Liu

Shanghai Key Laboratory of Materials Protection and Advanced Materials in Electric Power, College of Environmental and Chemical Engineering, Shanghai University of Electric Power, Shanghai 200090, China.

\*E-mail: [xuqunjie@shiep.edu.cn](mailto:xuqunjie@shiep.edu.cn); [laichunyan@shiep.edu.cn](mailto:laichunyan@shiep.edu.cn)

Received: 28 April 2017 / Accepted: 16 September 2017 / Published: 12 October 2017

---

Lithium-rich cathode material  $0.5\text{Li}_2\text{MnO}_3 \cdot 0.5\text{LiMn}_{1/3}\text{Ni}_{1/3}\text{Co}_{1/3}\text{O}_2$  for lithium-ion batteries has been successfully synthesized through a simple and mild method of precipitation reaction with mixed solvent. It crystallizes in a layered structure in the R-3m space group and the morphology of as-prepared sample has been investigated by the scanning electron microscopy (SEM) and transmission electron microscopy (TEM). The electrochemical testing results show that the as-prepared sample with 1:5 ratio of mixed distilled water-ethanol solvent delivers a initial discharge specific capacity of  $210.9 \text{mAh}\cdot\text{g}^{-1}$ , accompanying by the initial irreversible capacity loss of  $77 \text{mAh}\cdot\text{g}^{-1}$ , and a reversible capacity of  $167.1 \text{mAh}\cdot\text{g}^{-1}$  after 100 cycles at 1C between 2.0 and 4.8V. Furthermore, the sample prepared with 1:5 ratio of mixed distilled water-ethanol solvent exhibits a lower average discharge-voltage difference of 0.3895V from the 5th to 80th cycles, compared to the as-prepared sample without the addition of ethanol solvent (0.5188V). It means that the discharge voltage platform decreases slowly during repeated cycling and the surface structure of particles can be stabilized, owing to the mixed distilled water-ethanol solvent. According to the electrochemical impedance spectra and fitting results, the charge transfer resistance decreases from  $117.4 \Omega$  to  $85.7 \Omega$  and the lithium-ions diffusion coefficient value increases from  $2.06 \times 10^{-12} \text{cm}^2\cdot\text{s}^{-1}$  to  $6.05 \times 10^{-12} \text{cm}^2\cdot\text{s}^{-1}$ . These results testify to the superiority of as-prepared cathode material  $0.5\text{Li}_2\text{MnO}_3 \cdot 0.5\text{LiMn}_{1/3}\text{Ni}_{1/3}\text{Co}_{1/3}\text{O}_2$  in lithium-ion batteries.

---

**Keywords:** Lithium-ion batteries; Voltage fade;  $0.5\text{Li}_2\text{MnO}_3 \cdot 0.5\text{LiMn}_{1/3}\text{Ni}_{1/3}\text{Co}_{1/3}\text{O}_2$ ; Co-precipitation method; Mixed solvent

## 1. INTRODUCTION

Leveraging the advantages of lithium-ion batteries (LIBs), high energy density, environmental friendliness and long cycle-life, they are widely used in small electronic products, hybrid electric vehicles and smart grids. With the rapid development of electronic information technology, the requirements for lithium-ion batteries performance become higher. After a series of studies, layered lithium-rich cathode material  $0.5\text{Li}_2\text{MnO}_3 \cdot 0.5\text{LiMn}_{1/3}\text{Ni}_{1/3}\text{Co}_{1/3}\text{O}_2$ , with lower cost, higher discharge specific capacity and better thermal stability, compared with commercial cathode materials, has attracted wide attention from the researchers and been expected to be used on a large scale [1-3].

In recent years, based on the studies of charge-discharge mechanism for the  $0.5\text{Li}_2\text{MnO}_3 \cdot 0.5\text{LiMn}_{1/3}\text{Ni}_{1/3}\text{Co}_{1/3}\text{O}_2$  cathode material, the researchers find that a long irreversible platform appears when it is first charged to about 4.5V and the  $\text{Li}_2\text{MnO}_3$  component is activated via this platform to release a high specific capacity. Disappointingly, it is likely to be accompanied by the destruction of crystal structure, resulting in a large loss of capacity [4, 5]. During repeated cycling, the electrode polarization, which is triggered by the deterioration and side reaction of electrode/electrolyte, gives rise to gradual structural evolution from layered to spinel-like phase, resulting in voltage fade and weak cyclic performance [6, 7]. In view of the above disadvantages, the surface of  $0.5\text{Li}_2\text{MnO}_3 \cdot 0.5\text{LiMn}_{1/3}\text{Ni}_{1/3}\text{Co}_{1/3}\text{O}_2$  cathode materials can be modified to change its surface chemistry or provide a physical protective layer to stabilize the structure and improve the cyclic performance. There have many reports on the coating materials for the  $0.5\text{Li}_2\text{MnO}_3 \cdot 0.5\text{LiMn}_{1/3}\text{Ni}_{1/3}\text{Co}_{1/3}\text{O}_2$  cathode material, including oxides [8, 9], fluorides [10], phosphates [11, 12] and the like. However, the coating materials tend to accumulate on the surface of particles and could not be uniformly coated so that the uncovered surface of the particles is susceptible to HF in the electrolyte.

Herein, we introduce a mild and effective route, using different proportions of ethanol and distilled water as the mixed solvent, to synthesize the  $0.5\text{Li}_2\text{MnO}_3 \cdot 0.5\text{LiMn}_{1/3}\text{Ni}_{1/3}\text{Co}_{1/3}\text{O}_2$  materials. The structure and morphology are investigated extensively and the as-prepared materials exhibit high specific capacities and excellent cyclic performance when are used as cathode material for LIBs. The effect of mixed solvent on the electrochemical performance of lithium-rich cathode material is also discussed in detail. These advantages make  $0.5\text{Li}_2\text{MnO}_3 \cdot 0.5\text{LiMn}_{1/3}\text{Ni}_{1/3}\text{Co}_{1/3}\text{O}_2$  a promising cathode material for high performance lithium-ion batteries.

## 2. EXPERIMENTS

### 2.1. Synthesis of $0.5\text{Li}_2\text{MnO}_3 \cdot 0.5\text{LiMn}_{1/3}\text{Ni}_{1/3}\text{Co}_{1/3}\text{O}_2$ material

Layer-structured lithium-rich cathode materials  $0.5\text{Li}_2\text{MnO}_3 \cdot 0.5\text{LiMn}_{1/3}\text{Ni}_{1/3}\text{Co}_{1/3}\text{O}_2$  (denoted as LMNCO) were synthesized by a co-precipitation method. Stoichiometric amounts of lithium acetate ( $\text{LiCH}_3\text{COO} \cdot 2\text{H}_2\text{O}$ ), nickel acetate ( $\text{Ni}(\text{CH}_3\text{COO})_2 \cdot 4\text{H}_2\text{O}$ ), cobalt acetate ( $\text{Co}(\text{CH}_3\text{COO})_2 \cdot 4\text{H}_2\text{O}$ ), and manganese acetate ( $\text{Mn}(\text{CH}_3\text{COO})_2 \cdot 4\text{H}_2\text{O}$ ) were dissolved in the mixed distilled water/ethanol solvent at room temperature with ultrasonic shock (solution A). It should be noted that 5 mol% excessive lithium acetate was added to compensate for the loss of lithium during calcination and quench processes [13]. Ethylenediamine tetraacetic acid (denoted as EDTA) as precipitant was dissolved in

the mixed distilled water-ethanol solvent at 60 °C with ultrasonic shock (solution B). Solution A was added dropwise to solution B using a peristaltic pump with continuously violently stirring and the pH was controlled at 6. The brown flocculent precipitate was obtained when the metal-ions were fully reacted with EDTA, and then was transferred into blast oven without filter to evaporate water. The resulting powders was ground and then sintered in air at 800 °C for 16 hours with a heating rate of 5 °C·min<sup>-1</sup> to get the final LMNCO material.

The synthesis of the pristine LMNCO sample is based on distilled water as the solvent and the remaining steps are the same as above-mentioned. The proportions of mixed distilled water and ethanol solvent are 1: 1, 1: 5 and 1:10, respectively.

## 2.2. Structural analysis

The obtained LMNCO samples crystal structures were identified by X-ray powder diffraction (XRD) and the range of data acquisition was over 2 $\theta$  from 10° to 80° with a step size of 0.02° at a rate of 2°·min<sup>-1</sup>. The morphologies and size of as-prepared samples were characterized by a field emission scanning electron microscopy (FE-SEM, SU70) and transmission electron microscopy (TEM, JEOL JEM-2100).

## 2.3. Preparation of the electrodes and electrochemical methods

The electrochemical properties of the obtained cathode materials were evaluated in CR2032-type coin cells. The working electrode was obtained by mixing the as-prepared LMNCO active materials, acetylene black (as conductive agent) and the polyvinylidene fluoride (PVDF, as binder) with a weight ratio of 80:10:10 in N, N-dimethyl-pyrrolidone (NMP), and then stirring to form homogeneous slurry. The slurry was uniformly coated onto an aluminum foil (as current collector) and dried in a vacuum oven at 80 °C for 12 hours. After removal of the solvent (NMP), the obtained foil was rolled and punched into disks with the diameter of 14mm, followed closely by drying in vacuum at 80 °C. Then the electrolyte solution used was 1M LiPF<sub>6</sub> dissolved in a 1:1:1 mixture by volume of ethylene carbonate (EC), dimethyl carbonate (DMC) and ethylmethyl carbonate (EMC). And the cells was assembled from above-prepared working electrode, lithium metal foil (as counter electrode), polypropylene (Celgard 2400, as separator) and electrolyte solution in a vacuum glove box filled with argon gas (O<sub>2</sub> < 0.1ppm, H<sub>2</sub>O < 0.1ppm) at room temperature. The mass loading of active materials for all the cells was controlled at about 2.8 mg.

Galvanostatic cycling was tested in the potential window between 2.0V and 4.8V (vs. Li<sup>+</sup>/Li) on a LAND CT2001A battery test system (Wuhan Land, China) and the mass specific capacity is calculated by the mass of the active cathode materials. The cells cycled for 3 times at rate of 0.1C was subjected to electrochemical impedance spectroscopy (EIS) on a electrochemical work station (Chenhua CHI660e, Shanghai, China) with an amplitude voltage of 10mV and a frequency from 0.01 Hz to 100 kHz. Cyclic voltammetry (CV) testing was carried out on the same electrochemical work station in the potential window between 2.0V and 4.8V at a scanning rate of 0.1 mV·s<sup>-1</sup>. All electrochemical measurements were tested at room temperature (25 °C).

### 3. RESULTS AND DISCUSSION

#### 3.1. Structure and morphology

The XRD patterns of as-synthesized LMNCO samples via EDTA co-precipitation with different proportions of water-ethanol as the mixed solvent were showed in Figure 1. It can be seen that the peaks of as-prepared materials are sharp, manifesting excellent crystallinity, and most of diffraction peaks can be assigned to hexagonal  $\alpha$ - $\text{NaFeO}_2$  layered structure which belongs to the R-3m space group [14]. As the same step size and residence time are used to collect the XRD data of as-prepared materials, the diffraction peaks of the four materials are closely similar.

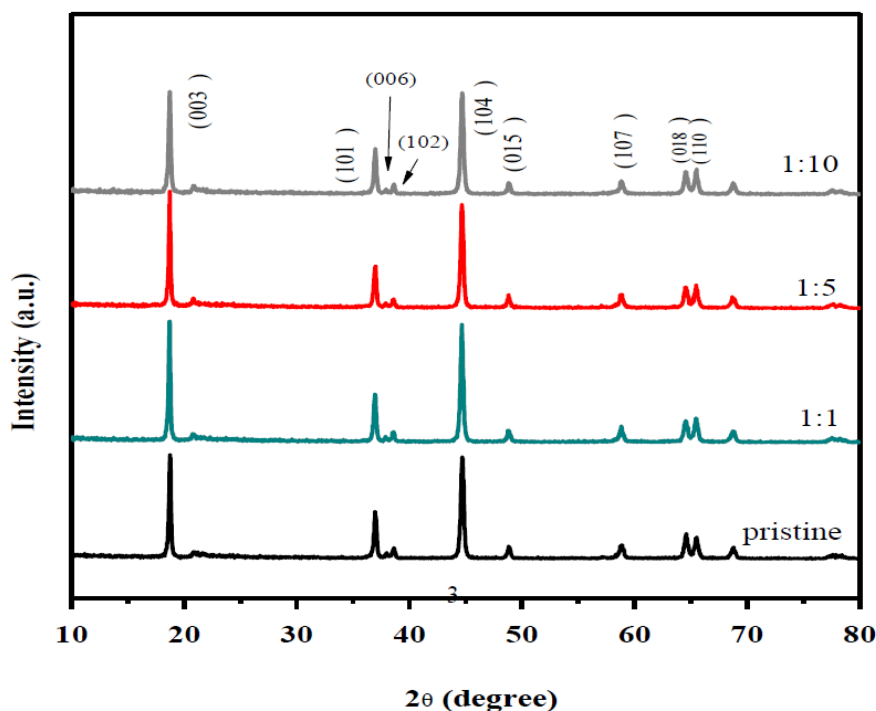


**Figure 1.** XRD patterns of as-prepared LMNCO samples.

There are no obvious impurity peaks on the XRD patterns with the addition of ethanol solvent, indicating that as-prepared materials are pure phase. The diffraction peaks at  $21^\circ$ - $25^\circ$  ( $2\theta$ ) are related to ordered arrangement of cations ( $\text{Li}^+$  and  $\text{Mn}^{4+}$ ) in the transition-metal layer ( $\text{LiMn}_6$ ), belonging to the characteristic diffraction peaks of  $\text{Li}_2\text{MnO}_3$  component with a  $C/2m$  space group. The degree of (006)/(102) and (108)/(110) splitting peaks is obvious, indicating that as-prepared samples have prominent lamellar properties [13, 15, 16].

In order to further investigate the effect of mixed solvent on the crystal structure for LMNCO samples, the material lattice parameters and the intensity ratio of the (003) and (104) major diffraction peaks are calculated and summarized in Table 1. When the intensity ratio is less than 1.2, it indicates that there is a serious cationic mixing phenomenon between the lithium-ion and the transition-metal ions. This phenomenon mainly occurs during the sintering process. The existence of cationic mixing

can be ignored while the ratio is greater than 1.2 [17, 18]. All the as-prepared samples have a much higher value than 1.2, and the value is the largest when the proportion of distilled water and ethanol is 1: 5. It is worth noting that the “c” value in the table 1 increases gradually with the addition of ethanol solvent and the values of synthesized samples with mixed solvent are larger than that of the pristine sample, indicating increased inter-slab distance. The materials inter-slab distance enlargement facilitates better lithium-ions insertion/extraction and leads to a faster electrochemical process. The ratios of all synthesized samples  $c/a$  are higher than 4.9, which indicated that all synthesized materials have good layer crystal structure. As we all known that a larger  $c/a$  value suggests a better hexagonal structure [19, 20].

**Table 1.** Lattice parameters of as-prepared LMNCO samples.

	a	c	c/a	$I_{(003)}/I_{(104)}$
pristine	0.2879	1.4183	4.9264	1.3680
1:1	0.2852	1.4227	4.9884	1.3504
1:5	0.2850	1.4228	4.9923	1.4472
1:10	0.2855	1.4246	4.9898	1.4121

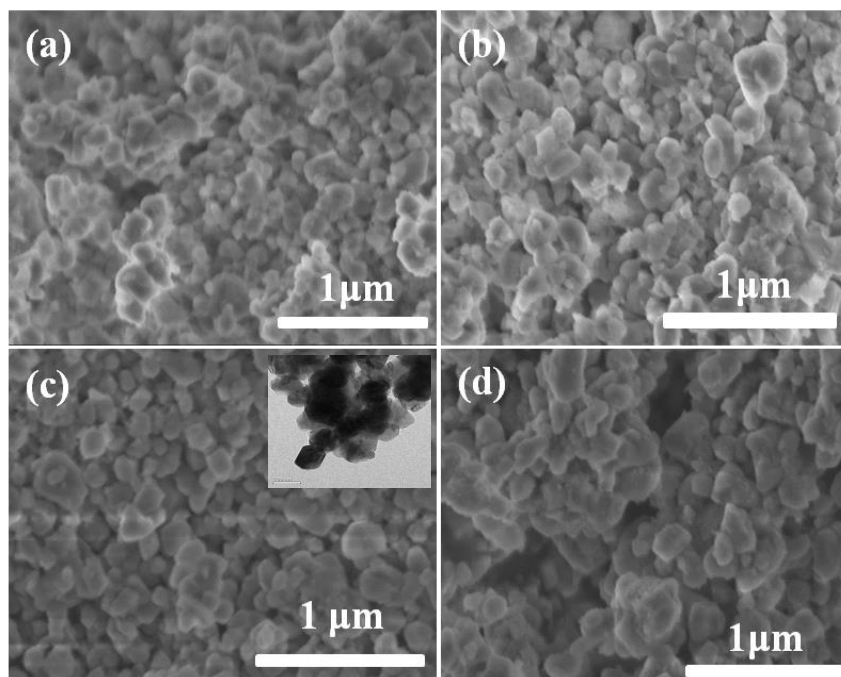
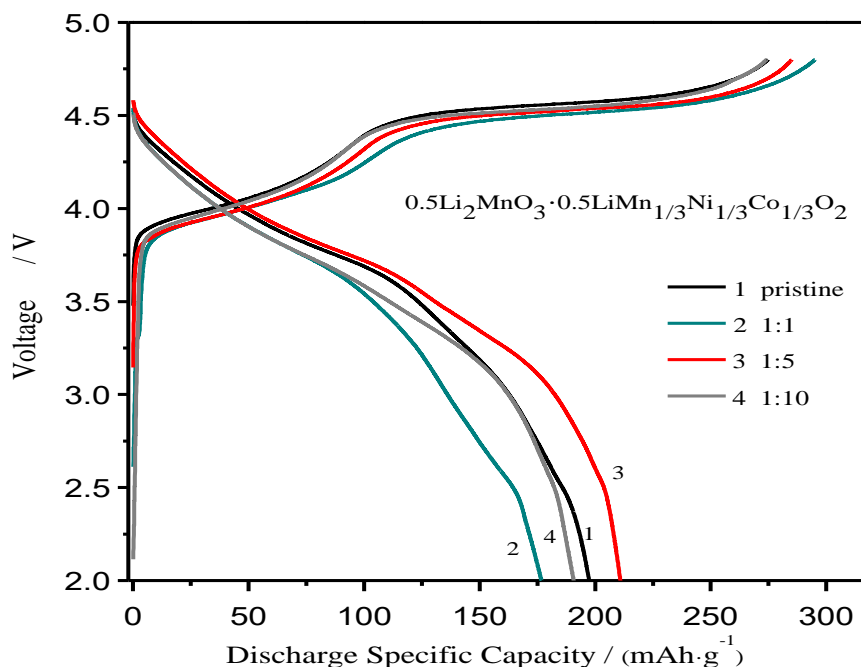


**Figure 2.** SEM images of as-prepared LMNCO samples: (a) pristine; (b)1:1; (c)1:5; (d) 1:10.

The SEM images of LMNCO samples are shown in Figure 2. Figure 2(a) reveals that the pristine sample is composed of irregular polygonal particles with diameters in a wide range of 300-

800nm and the agglomeration between particles is serious. When ethanol is added to the distilled water to form mixed solvent, the particles turn to be monodispersed in a circular or elliptical shape, with sharp edges and smooth planes, suggesting that LMNCO samples are highly crystallized (Figure 2(b) and (c)). Especially for the sample prepared with proportion of 1:5, the distribution of particles is the most uniform and the agglomeration between particles can be ignored. It can be seen from the Figure 2(c) that TEM images of the as-prepared sample with proportion of 1:5, the size of particles is smaller than pristine sample within 100-400nm. The primary reason for the differences in the morphology of all particles should be ascribed to the addition of ethanol, which plays a role of surfactant in the preparation process to change the surface structure and state of the particles, resulting the dispersibility of particles is improved. However, when the amount of ethanol is further increased, the agglomeration of LMNCO sample has not been alleviated (as shown in Figure 2(d)) and the particles become larger. This is possibly caused by complex physical changes between the particles owing to more ethanol solvents [21].

### 3.2. Charge and discharge performance



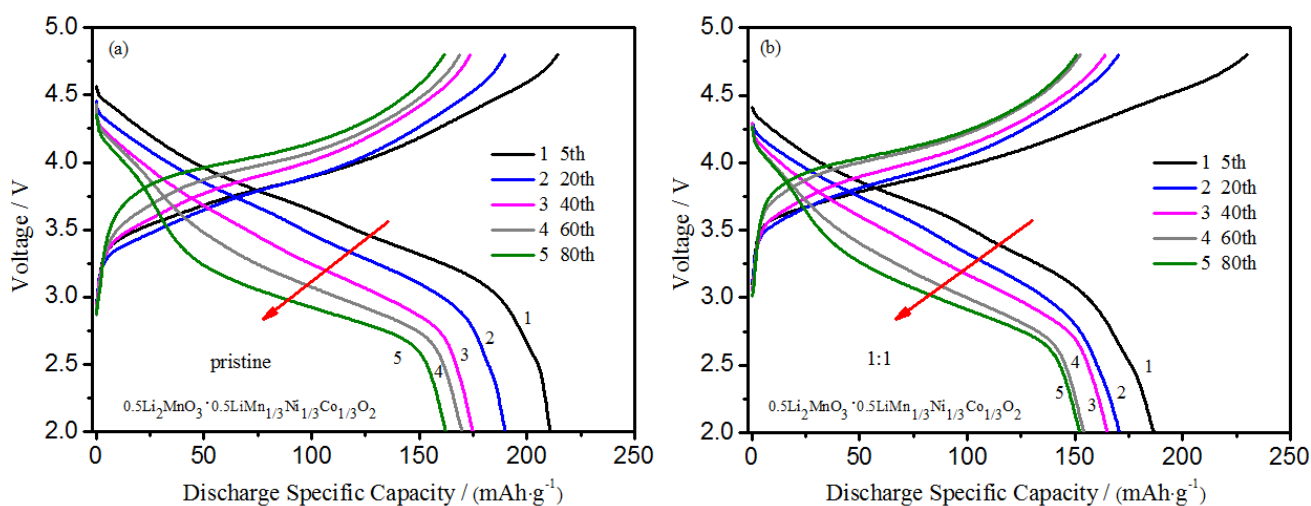
**Figure 3.** Typical initial charge and discharge curves of as-prepared samples.

Figure 3 showed the initial charge-discharge curves of as-synthesized LMNCO samples at a rate of 1C in the voltage range of 2.0-4.8V at room temperature. As shown in Figure 3, when the charge potential is no more than 4.5V (vs.  $\text{Li}^+/\text{Li}$ ), the charging curves of the four samples display the slope area. This slope area could be ascribed to the nickel ions and cobalt ions in the  $\text{LiMn}_{1/3}\text{Ni}_{1/3}\text{Co}_{1/3}\text{O}_2$  component are oxidized to +4 valence, accompanied by  $\text{Li}^+$  deintercalation from

the layered structure. When the charge potential reaches 4.5V (vs.  $\text{Li}^+/\text{Li}$ ), a long characteristic voltage platform appears, which could be attributed to the activation of  $\text{Li}_2\text{MnO}_3$  component, showing a large charge specific capacity. At the same time, the oxygen ions are easily removed from  $\text{Li}_2\text{MnO}_3$  component and this process is irreversible leading to a large loss of initial capacity [22, 23].

The initial discharge specific capacities of as-prepared samples with the proportions of mixed distilled water-ethanol solvent are 1:1, 1:5, 1:10 are  $176.8 \text{ mAh}\cdot\text{g}^{-1}$ ,  $210.9 \text{ mAh}\cdot\text{g}^{-1}$ ,  $190.7 \text{ mAh}\cdot\text{g}^{-1}$ , respectively, and that of pristine sample is  $197.3 \text{ mAh}\cdot\text{g}^{-1}$ . With similar charge capacities, the initial irreversible capacities loss of four samples are  $82.9 \text{ mAh}\cdot\text{g}^{-1}$  (pristine),  $121 \text{ mAh}\cdot\text{g}^{-1}$  (1:1),  $77 \text{ mAh}\cdot\text{g}^{-1}$  (1:5) and  $86.2 \text{ mAh}\cdot\text{g}^{-1}$  (1:10). It is clear that the addition of ethanol solvent has a significant effect on the initial irreversible capacity loss of the LMNCO material. Especially when the mixture ratio of distilled water-ethanol is 1:5, the as-prepared sample provides the lowest initial irreversible capacity loss.

For layered lithium-rich cathode material, the voltage platform tends to drop down during the repeated discharge process, namely the voltage fade, resulting in inferior energy density and cycle stability. Figure 4 shows the discharge profile evolutions for the 5th, 20th, 40th, 60th, 80th cycles of four samples at a rate of 1C in the voltage window between 2.0V and 4.8V (vs.  $\text{Li}^+/\text{Li}$ ). It is obvious that the voltage platform of all samples are declining from the 5th to 80th cycles, demonstrating that the polarization of electrode is prone to be more and more serious during cycling. In addition, the primary reason for the voltage fade can be assigned to the structure rearrangement caused by gradual structure evolution from layered to spine-like phase during cycling [24, 25]. Firstly, the transition-metal ions easily occupy the oxygen vacancies formed during the initial charge-discharge cycle, and lithium-ions migrate to the tetrahedral sites, resulting in distortion of oxygen lattices. Thereafter, when a large amount of lithium-ions remove from tetrahedral sites at high voltage, the transition-metal ions migrate to the octahedral sites in the Li layer through the adjacent tetrahedral position, which promotes the formation of spine-like phase[26-29].



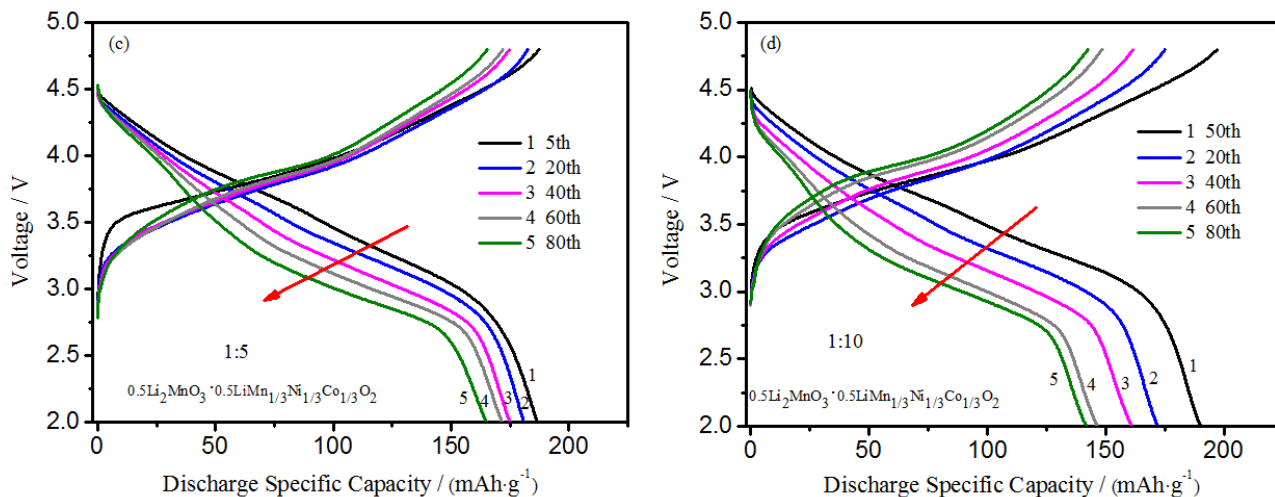


**Figure 4.** The voltage profiles of the as-prepared LMNCO samples at the 5th, 20th, 40th, 60th, 80th cycles

The more cycles, the thicker the layer of structure rearrangement, owing to extensive migration of the transition-metal ions into the Li layer. In comparison with the graphs (a), (b), (c) and (d) in Figure 4, it can be found that the tendency of the discharge voltage platform for the LMNCO samples is slowing down with the continuous addition of the ethanol solvent, indicating that the surface structure of particles can be stabilized to a certain extent.

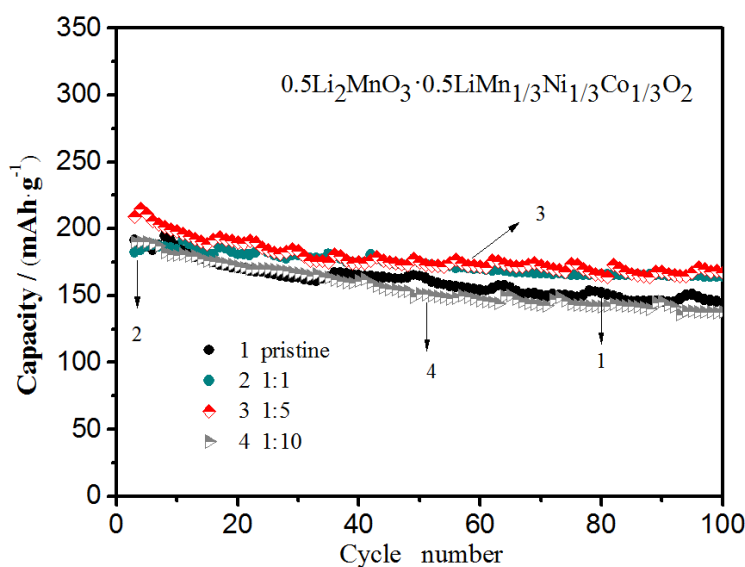


**Figure 5.** Cycling behavior of as-prepared samples.

In principle, the cationic mixing limits the intercalation/deintercalation of lithium-ions, which is mainly related to the insertion/migration of octahedral sites in the structure of layered-spinel, corresponding to the value of  $I_{(003)}/I_{(104)}$  in the above XRD analysis. When the transition-metal ions

continue occupying the vacancies in the Li layer, the vacant octahedral sites can be reversible embedded and removed Li ions in the subsequent cycles. It is clear that the addition of ethanol solvent in the preparation process is not conducive to the formation of spinel phase. The differences of average discharge voltage are 0.5188V (pristine), 0.4018V (1:1), 0.3895V (1:5), and 0.5872V (1:10) from the 5th to 80th cycles. Obviously, when the ratio of distilled water-ethanol is 1: 5, the discharge voltage platform of LMNCO sample decreased most slowly.

The cycling behavior of as-prepared LMNCO samples further highlight the advantages of mixed solvent, as shown in Figure 5. All samples were cycled at a rate of 1C between 2.0 and 4.8V. Overall, the discharge capacities are gradually reduced during repeated cycling, due to the dissolution of the LMNCO active materials in the electrolyte or any other side reaction. After 100 cycles, the LMNCO samples delivers discharge specific capacities of 144.4 mAh·g<sup>-1</sup> (pristine), 158.1 mAh·g<sup>-1</sup> (1:1), 167.1 mAh·g<sup>-1</sup> (1:5), and 137.2 mAh·g<sup>-1</sup> (1:10), respectively. It is obvious that the as-prepared samples exhibit the highest capacity and most prominent cyclic performance when the proportion of distilled water-ethanol is 1:5, compared with other samples. It can be concluded that the addition of ethanol solvent to form mixed solvent could reduce agglomeration between particles and shorten the channels for lithium-ions to migration, thereby enhancing the ability of lithium-ions to intercalate/deintercalate. These conclusions echo the SEM images of the four samples and the increase of “c” value in the XRD analysis.

### 3.3. Cyclic voltammetry

In order to further investigate and compare the electrochemical performances of the samples with or without the addition of ethanol, the initial three CV curves of as-prepared samples at a slow scanning rate of 0.1 mV·s<sup>-1</sup> in voltage range of 2V-4.8V (vs. Li<sup>+</sup>/Li) were illustrated in Figure 6.

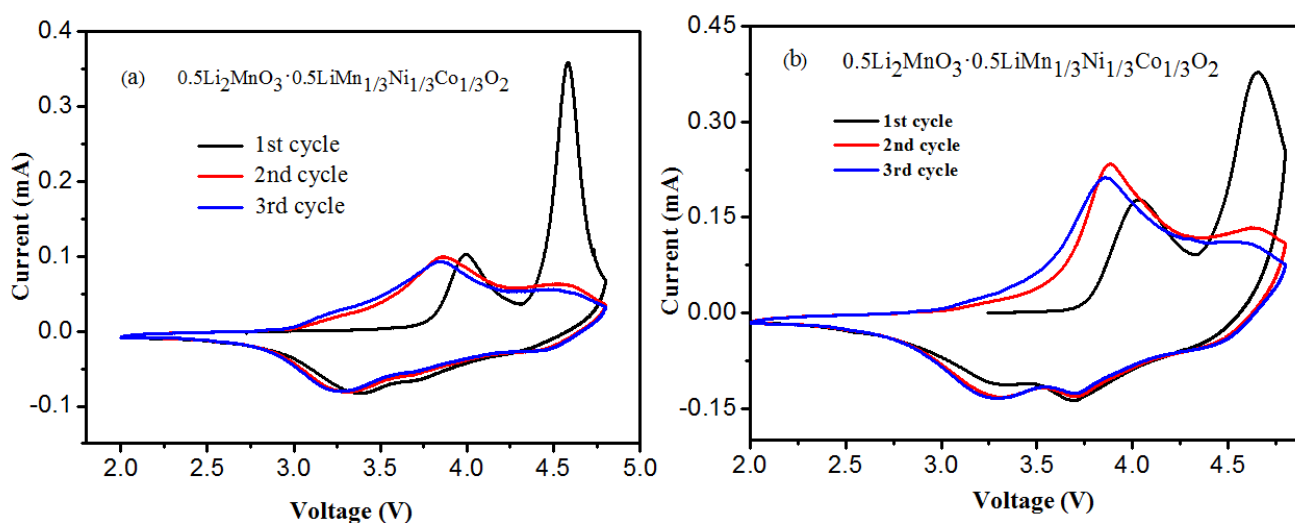


**Figure 6.** CV curves of as-prepared LMNCO samples: (a) pristine and (b) 1:5.

On the whole, the anodic peaks appeared in the first cycle are obviously different from those in the 2nd and 3rd cycle, which is related to the unique charge-discharge mechanism for the lithium-rich electrode materials. During the first cycle, the anodic peak near 4.1V corresponds to the removal of  $\text{Li}^+$  from the  $\text{LiMn}_{1/3}\text{Ni}_{1/3}\text{Co}_{1/3}\text{O}_2$  component, accompanied by the oxidation process of  $\text{Ni}^{2+}/\text{Ni}^{4+}$  and  $\text{Co}^{3+}/\text{Co}^{4+}$ . The sharp anodic peak at  $\sim 4.6\text{V}$  represents the activation process of  $\text{Li}_2\text{MnO}_3$  component after  $\text{Li}$  ions are extracted in the form of  $\text{Li}_2\text{O}$ , which means inactive  $\text{Li}_2\text{MnO}_3$  becomes active  $[\text{MnO}_2]$  [30]. It should be noted that the higher the anodic peak (near  $4.6\text{V}$ ) current, the more excellent the kinetic performance of samples. These two anodic peaks (at  $\sim 4.1\text{V}$  and  $\sim 4.6\text{V}$ ) correspond to the slope area and characteristic platform in the initial charge and discharge curves. Moreover, in the 2nd and 3rd cycle, the peaks near  $3.3\text{V}$ ,  $3.7\text{V}$  and  $4.4\text{V}$  can be attributed to the reduction of  $\text{Mn}^{4+}$ , the insertion of  $\text{Li}^+$  into the  $\text{MnO}_2$  structure and the reduction process of  $\text{Ni}^{2+}$  and  $\text{Co}^{3+}$  of layered  $\text{LiMn}_{1/3}\text{Ni}_{1/3}\text{Co}_{1/3}\text{O}_2$  structure, respectively [31-33], suggesting that the activation of the  $\text{Li}_2\text{MnO}_3$  region is irreversible.

Compared with the first cycle, the intensity of peaks in the second and third curves decreases and the peaks potential is shifted, indicating that the extensive loss of specific capacity and irreversible phase transformation prevented lithium-ions from migrating. However, the symmetrical curves in the 2nd and 3rd cycle exhibit good coincidence, which means that the lithium-ions of as-prepared LMNCO samples could be reversibly embedded and removed. Although the CV curves of these two samples have similar shapes, it can be found that the peak current corresponding to the oxidation peak at  $4.6\text{V}$  is about  $0.3776\text{ mA}$  for the sample prepared with a 1:5 ratio of distilled water-ethanol, higher than pristine sample ( $0.3542\text{ mA}$ ), which indicates better electrochemical performance. This results square with the electrochemical performance obtained above.

### 3.4. Electrochemical Impedance Spectroscopy

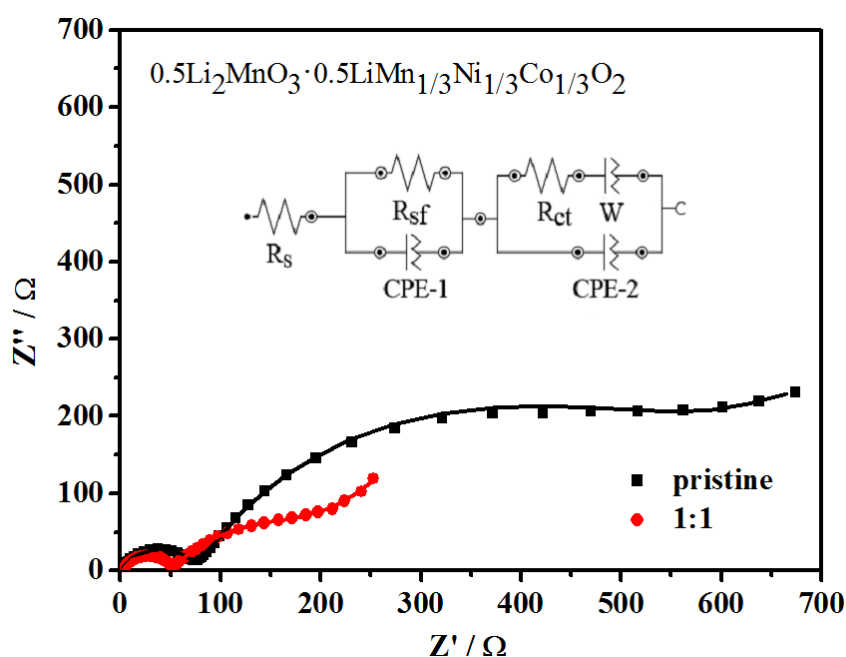


**Figure 7.** Nyquist plots measured for as-prepared LMNCO samples after 3 cycles.

Electrochemical impedance spectroscopy (EIS) is very useful for evaluating kinetic and interfacial parameters. The Nyquist plots of the LMNCO samples are collected at charge state of 4.8V under frequency of 0.01 Hz-100 kHz during charge with LMNCO electrodes after 3 cycles at a rate of 0.1 C within the potential range of 2.0-4.8V, as shown in Figure 7. At the same time, the inset in Figure 7 showed their equivalent circuit model, where  $R_s$  and  $R_{sf}$  represent the solution resistance and the resistance of solid electrolyte interface film (SEI film) respectively,  $R_{ct}$  refers to the charge transfer resistance, CPE-1 and CPE-2 are related to the constant phase angle, and  $W_s$  is the Warburg diffusion impedance.

The impedance spectra of the samples (presented as Nyquist plots) usually comprise three features: two semicircular arcs and a straight line. The semicircular arc at high frequency region can be considered as the migration of lithium-ions in the SEI film and the semicircular arc at medium-low frequency is usually arisen from the charge transfer process, corresponding to the charge transfer resistance ( $R_{ct}$ ). The straight line in the low frequency region refers to the solid-state diffusion of lithium-ions through the bulk of active material, reflecting the lithium-ions diffusion Warburg resistance [34, 35]. The impedance spectra revealed an obvious decrease in these impedance semicircles, suggesting that the barrier of the charge transfer reaction at the electrode/electrolyte is removed, which can be assigned to the surface effect on shortening lithium-ions diffusion pathways with mixed solvent. According to the parameters obtained from the fitting results as shown in Table 2, it can be found that the sample prepared with the 1:5 ratio of mixed distilled water-ethanol solvent has lower  $R_{ct}$  value and higher  $D_{Li}$  compared with pristine sample, demonstrating that the rate of  $Li^+$  diffusion in the former sample is drastically increased during cycling by mitigating agglomeration between particles.

**Table 2.** Parameters of fitting results derived from the equivalent circuit model for as-prepared LMNCO samples.

	$R_s / \Omega$	$R_{sf} / \Omega$	$R_{ct} / \Omega$	$D_{Li} / \text{cm}^2 \cdot \text{s}^{-1}$
pristine	2.76	71.8	117.4	$2.06 \times 10^{-12}$
1:1	2.35	55.4	85.7	$6.05 \times 10^{-12}$

#### 4. CONCLUSIONS

In this article, layered  $0.5\text{Li}_2\text{MnO}_3 \cdot 0.5\text{LiMn}_{1/3}\text{Ni}_{1/3}\text{Co}_{1/3}\text{O}_2$  cathode material has been successfully synthesized via a EDTA co-precipitation method combined with different proportions of mixed distilled water-ethanol solvent. The structure and morphology of the sample prepared with 1:5 ratio of mixed distilled water-ethanol solvent were characterized by XRD and SEM, which showed favourable crystallinity and dispersibility compared to pristine sample. The relative improvements of

as-prepared samples, as cathode material in LIBs, were achieved in cycling performance at high cutoff voltage of 4.8V. Particularly, the sample prepared with 1:5 ratio of mixed distilled water-ethanol solvent exhibited a minor initial irreversible capacities loss of 77 mAh·g<sup>-1</sup> and a average discharge voltage of 0.3895 V from the 5th to 80th cycles, compared to that of pristine sample (82.9 mAh·g<sup>-1</sup>, 0.5188V). It is indicated that the discharge voltage platform decreased slowly during repeated cycling and the surface structure of particles can be stabilized to a certain extent. Furthermore, the EIS study showed that 0.5Li<sub>2</sub>MnO<sub>3</sub>·0.5LiMn<sub>1/3</sub>Ni<sub>1/3</sub>Co<sub>1/3</sub>O<sub>2</sub> cathode material prepared with 1:5 ratio of mixed solvent has also surface effect on shortening lithium-ions diffusion pathways, revealing small charge transfer resistance (85.7Ω) and large lithium-ions diffusion coefficient value (6.05×10<sup>-12</sup> cm<sup>2</sup>·s<sup>-1</sup>). On the basis of this work, EDTA co-precipitation method with mixed distilled water-ethanol solvent would be a promising synthetic method for high-performance LIBs toward practical applications in the future.

#### ACKNOWLEDGMENTS

This research was financially supported by Shanghai Science and Technology Committee (Grant number 16020500800).

#### References

1. C. S. Johnson, N. C. Li, C. Lefief, J. T. Vaughey, M. M. Thackeray, *Chem. Mater.*, 20 (2008) 6095–6106.
2. J. S. Kim, C. S. Johnson, J. T. Vaughey, M. M. Thackeray, *Chem. Mater.*, 16 (2004) 1996-2006.
3. W. Liu, P. Oh, X. Liu, M. J. Lee, W. Cho, S. Chae, Y. Kim, J. Cho, *Angew. Chem.*, 54 (2015) 4440-4457.
4. W. C. West, J. Soler, M. C. Smart, B. V. Ratnakumar, S. Firdosy, V. Ravi, M. S. Anderson, J. Hrbacek, E. S. Lee, A. Manthiram, *J. Electrochem. Soc.*, 158 (2011) A883.
5. H. J. Yu, H. Kim, Y. Wang, P. He, D. Asakura, Y. Nakamura, H. S. Zhou, *Phys. chem. chem. phys.*, 14 (2012) 6584-6595.
6. H. J. Yu, H. S. Zhou, *J. Phys. Chem. Lett.*, 4 (2013) 1268-1280.
7. J. M. Zheng, M. Gu, A. Genc, J. Xiao, P. H. Xu, X. L. Chen, Z. H. Zhu, W. B. Zhao, L. Pullan, C. M. Wang, J. G. Zhang, *Nano lett.*, 14 (2014) 2628-2635.
8. X. F. Zhang, I. Belharouak, L. Li, Y. Lei, J. W. Elam, A. Nie, X. Q. Chen, R.S. Yassar, R. L. Axelbaum, *Adv. Ene. Mat.*, 3 (2013) 1299-1307.
9. X. L. Yuan, Q. J. Xu, X. N. Liu, H. M. Liu, Y. L. Min, Y. Y. Xia, *Electrochim. Acta*, 213 (2016) 648-654.
10. H. B. Kim, B. C. Park, S. T. Myung, K. Amine, J. Prakash, Y. K. Sun, *J. Power Sources*, 179 (2008) 347-350.
11. J. Cho, H. Kim, B. Park, *J. Electrochem. Soc.*, 151 (2004) A1707.
12. X. L. Ma, C. W. Wang, X. Y. Han, J. T. Sun, *J. Alloy. Compd.*, 453 (2008) 352-355.
13. X. L. Yuan, Q. J. Xu, C. Wang, X. N. Liu, H. M. Liu, Y. Y. Xia, *J. Power Sources*, 279 (2015) 157-164.
14. Y. D. Zhang, Y. Li, X. Q. Niu, D. H. Wang, D. Zhou, X. L. Wang, C. D. Gu, J. P. Tu, *J. Mater. Chem. A*, 3 (2015) 14291-14297.
15. B. H. Song, M. O. Lai, L. Lu, *Electrochim. Acta*, 80 (2012) 187-195.
16. Y. Cho, S. Lee, Y. Lee, T. Hong, J. Cho, *Adv. Ene. Mat.*, 1 (2011) 821-828.

17. J. T. Liu, S. B. Wang, Z. P. Ding, R. Q. Zhou, Q. B. Xia, J. F. Zhang, L. B. Chen, W. F. Wei, P. Wang, *ACS appl. mater. interfaces*, 8 (2016) 18008-18017.
18. B. H. Song, S. J. Day, T. Sui, L. Lu, C. C. Tang, A.M. Korsunsky, *Phys. chem. chem. phys.*, 18 (2016) 4745-4752.
19. B. Li, C. Li, Z. L. Cao, Z. H. Yang, S. L. Liu, X. M. Fan, F. Chen, Y. Tian, W. B. Zhang, S. H. Yang, M. Li, *RSC Adv.*, 6 (2016) 31014-31018.
20. Y. F. Chen, K. Xie, C. M. Zheng, Z. Y. Ma, Z. X. Chen, *ACS appl. mater. interfaces*, 6 (2014) 16888-16894.
21. G. Ma, S. Li, W. X. Zhang, Z. H. Yang, S. L. Liu, X. M. Fan, F. Chen, Y. Tian, W. B. Zhang, S. H. Yang, M. Li, *Angew. Chem.*, 55 (2016) 3667-3671.
22. Y. Jiang, Z. Yang, W. Luo, X. L. Hu, W. X. Zhang, Y. H. Huang, *J. Mater. Chem.*, 22 (2012) 14964.
23. J. Tian, Y. F. Su, F. Wu, S. Y. Xu, F. Chen, R. Chen, Q. Li, J. H. Li, F. C. Sun, S. Chen, *ACS appl. mater. interfaces*, 8 (2016) 582-587.
24. M. Gu, I. Belharouak, J. Zheng, H. Wu, J. Xiao, A. Genc, K. Amine, S. Thevuthasan, D. R. Baer, J. G. Zhang, N. D. Browning, J. Liu, C. Wang, *ACS Nano*, 7 (2013) 760-767
25. J. Hong, D. H. Seo, S. W. Kim, H. Gwon, S. T. Oh, K. Kang, *J. Mater. Chem.*, 20 (2010) 10179.
26. J. M. Zheng, P. H. Xu, M. Gu, J. Xiao, N. D. Browning, P. F. Yan, C. M. Wang, J. G. Zhang, *Chem. Mater.*, 27 (2015) 1381-1390.
27. B. Xu, C. R. Fell, M. F. Chi, Y. S. Meng, *Energy Environ. Sci.*, 4 (2011) 2223.
28. C. S. Johnson, N. C. Li, C. Lefief, J. T. Vaughey, M. M. Thackeray, *Chem. Mater.*, 20 (2008) 6095-6106.
29. J. R. Croy, D. Kim, M. Balasubramanian, K. Gallagher, S. H. Kang, M. M. Thackeray, *J. Electrochem. Soc.*, 6 (2012) A781-A790.
30. J. Lim, S. Lee, K. Suzuki, K. Kim, S. Kim, S. Taminato, M. Hirayama, Y. Oshima, K. Takayanagi, R. Kanno, *J. Power Sources*, 279 (2015) 502-509.
31. F. Wu, N. Li, Y. F. Su, H. F. Shou, L. Y. Bao, W. Yang, L. J. Zhang, R. An, S. Chen, *Adv. mater.*, 25 (2013) 3722-3726.
32. J. Zhang, Z. H. Lei, J. L. Wang, Y. N. NuLi, J. Yang, *ACS appl. mater. interfaces*, 7 (2015) 15821-15829.
33. X. Jin, Q. J. Xu, H. M. Liu, X. N. Yuan, Y. Y. Xia, *Electrochim. Acta*, 136 (2014) 19-26.
34. L. J. Zhang, W. Borong, L. Ning, W. Feng, *Electrochim. Acta*, 118 (2014) 67-74.
35. E. S. Lee, A. Huq, A. Manthiram, *J. Power Sources*, 240 (2013) 193-203.